Nephrol Dial Transplant (2021) 36: 1006–1016
doi: 10.1093/ndt/gfab014
Advance Access publication 5 February 2021

ORIGINAL ARTICLE

Increased dishevelled associated activator of morphogenesis 2, a new podocyte-associated protein, in diabetic nephropathy

Chenyang Qi[1,2], Faten Alsomali[3], Jinyong Zhong[2,4], Raymond C. Harris[5], Valentina Kon[4], Haichun Yang[2,4] and Agnes B. Fogo[2,4,5]

[1]Department of Pathology, School of Basic Medical Sciences, Shanghai Medical College, Fudan University, Shanghai, China, [2]Department of Pathology, Microbiology and Immunology, Vanderbilt University Medical Center, Nashville, TN, USA, [3]College of Medicine, Alfaisal University, Riyadh, Saudi Arabia, [4]Division of Pediatric Nephrology, Vanderbilt University Medical Center, Nashville, TN, USA and [5]Division of Nephrology, Vanderbilt University Medical Center, Nashville, TN, USA

Correspondence to: Agnes B. Fogo; E-mail: agnes.fogo@vumc.org

ABSTRACT

Background. Previously, by using proteomic analysis and RNA sequencing in isolated glomeruli, we identified several novel differentially expressed proteins in human and mouse diabetic nephropathy (DN) versus controls, including dishevelled associated activator of morphogenesis 2 (DAAM2). DAAM2 binds the Wnt effector Dvl. We aimed to study possible contributions of DAAM2 to DN.

Methods. We assessed DAAM2 by immunostaining in non-cancer regions of human nephrectomy (Nx), DN and normal donor kidney tissues. We also examined DAAM2 in DN mice (*db*/*db* eNOS$^{-/-}$) and Nx mice. DN mice treated with angiotensin-converting enzyme inhibitor (ACEI), dipeptidyl peptidase 4 inhibitor (DPP4I) or vehicle were compared. DAAM2 was knocked down in primary cultured podocytes by small interfering RNA to study its effects on cell function.

Results. In normal human glomeruli, DAAM2 was expressed only on podocytes. DAAM2 expression was increased in both Nx and DN versus normal donors. Podocyte DAAM2 expression was increased in DN and Nx mouse models. Glomerular DAAM2 expression correlated with glomerular size and was decreased significantly by ACEI while DPP4I only numerically reduced DAAM2. In primary cultured podocytes, knockdown of DAAM2 enhanced adhesion, slowed migration, activated Wnt–β-catenin signaling and downregulated mammalian target of rapamycin complex 1 (mTORC1) and Rho activity.

Conclusions. Podocyte DAAM2 is upregulated in both Nx and DN, which could be contributed to by glomerular hypertrophy. We hypothesize that DAAM2 regulates podocyte function through the mTORC1, Wnt/β-catenin and Rho signaling pathways.

Keywords: DAAM2, diabetic nephropathy, glomerular hypertrophy, nephrectomy, podocytes

INTRODUCTION

Diabetic nephropathy (DN) is the leading cause of end-stage renal disease worldwide. However, the underlying pathogenic mechanisms of progression of human DN are still not clear [1, 2]. We previously compared human normal versus DN glomerular samples by mass spectrometry and identified differentially expressed proteins. Furthermore, we assessed differentially expressed glomerular genes in *db*/*db* eNOS$^{-/-}$ (DN model) versus eNOS$^{-/-}$ (non-diabetic control) mice by RNA sequencing and identified genes correlated with the progression of DN at 18 weeks in mice [3]. By comparing the proteins mined in human kidney tissue and the differentially expressed genes in mice, we identified potential targets of interest. In this study we focused on one of these genes, *DAAM2*, which codes the dishevelled (Dvl) associated activator of morphogenesis 2 protein and is expressed in glomeruli. DAAM2 belongs to the DAAM protein family, which binds to the Wnt effector Dvl [4]. DAAM1 and DAAM2 share conserved formin homology and GTPase protein binding domains, which suggests a role in cell motility by recruiting the actin-capping protein profilin and catalyzing the assembly of unbranched actin filaments [5, 6]. DAAM1 has been extensively studied during embryonic development. Non-canonical Wnt/Rho/planar cell polarity (PCP) pathway signaling causes Dvl to bind DAAM1, which increases its affinity for RhoA and promotes actin assembly [4]. Due to its function in nucleation of unbranched actin filaments and in cytoskeletal organization through the PCP pathway [7], DAAM1 regulates cell polarity, motility and migration during morphogenesis and organogenesis in various epithelial cells, oocytes, sperms and cancer cells [8]. However, the role of DAAM2 remains undefined. There are only a few studies, most in the neuromuscular system or in embryonic development, indicating the following functions and related pathways of DAAM2 [9]. DAAM2 is co-

required with DAAM1 for myocardial maturation and sarcomere assembly by inhibiting β-catenin activity and maintaining AKT activity without affecting Rho [10]. DAAM2 is required for canonical Wnt signaling during patterning in the dorsal spinal cord, functioning through the clustering and formation of Wnt receptor signalosomes through the PIP5K–PIP2 axis [11]. DAAM2 also mediates adhesion at cell junctions by physically interacting with α-catenin and N-cadherin driven by the Pitx2–Wnt5 pathway, which causes left condensation and asymmetric gut morphogenesis [12]. These findings suggest DAAM2 affects the canonical Wnt–β-catenin signaling pathway. DAAM2 also promotes Wnt5a-induced Rho activation and the bone-resorbing activity of osteoclasts, which involves a non-canonical Wnt–PCP pathway [13]. The kidney shows expression of DAAM2. However, the exact contribution of DAAM2 to renal disease has not been elucidated.

In this study we assessed DAAM2 locations and expression in normal and diseased kidney. We further studied DAAM2 effects on podocyte function through several signaling pathways.

MATERIALS AND METHODS

Human samples

We studied 9 cases from healthy donors, 20 cases of non-cancer regions of human nephrectomy (Nx) and 60 cases of biopsy-proven DN (Classes II, III and IV; 20 cases per class, by Tervaert class) [14]. Human data collection followed protocols approved by the Institutional Review Board at Vanderbilt University Medical Center.

Mice samples

A total of nine wild-type (WT) C57BLKS/J mice (six male and three female), nine WT eNOS$^{-/-}$ (seven male and two female) and nine *db*/*db* eNOS$^{-/-}$ mice (six male and three female) were used in the study. All procedures were approved by the Vanderbilt University Medical Center Institutional Animal Care and Use Committee. Additional *db*/*db* eNOS$^{-/-}$ mice were treated with dipeptidyl peptidase 4 inhibitor (DPP4I; 3 mg/kg body weight in diet; $n = 6$), angiotensin-converting enzyme inhibitor (ACEI; 50 mg/L in drinking water; $n = 6$) or both starting at 10 weeks of age until the mice were sacrificed at 18 weeks of age.

WT S129/Sv mice underwent uninephrectomy (uniNx), 5/6 Nx or sham Nx at 10 weeks of age as previously described [15]. Mice were followed for 9 weeks after Nx or 5/6 Nx and then euthanized. Urine and serum were collected at intervals. Kidneys were harvested and fixed in 4% paraformaldehyde (PFA).

Blood and urinary measurements

Systolic blood pressure was measured by a tail-cuff blood pressure monitor (model 2000, Muromachi Kikai, Tokyo, Japan) in conscious trained mice. Spot urinary albumin was determined using Albuwell M kits (Exocell, Philadelphia, PA, USA). Urine creatinine was measured using the QuantiChrom Creatinine Assay Kit (BioAssay Systems, Hayward, CA, USA).

Morphological assessment and immunohistochemistry

Kidney tissue was immersion fixed in 4% PFA and routinely processed and 3-μm sections were stained with periodic acid–Schiff. Individual glomerulus area was measured by image analyzing software (AxioVision; Carl Zeiss, Dublin, CA, USA) and

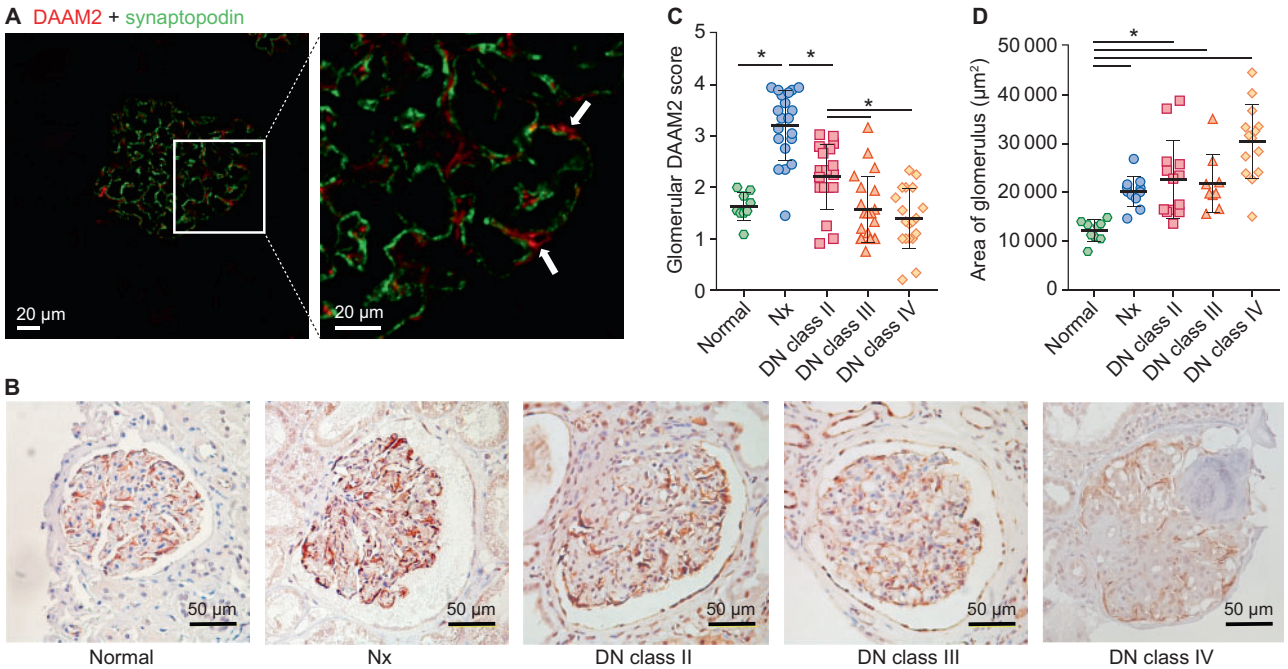

FIGURE 1: Increased podocyte DAAM2 in human DN biopsies and Nx specimens. (**A**) Double staining (red: DAAM2; green: synaptopodin) shows glomerular DAAM2 expression in podocytes in normal glomerulus. (**B** and **C**) Podocyte DAAM2 increased in Nx and DN Class I versus normal kidney and was less in DN Classes III and IV. (**D**) Glomerular size increased in Nx and DN versus normal kidney.

Table 1. Clinical characteristics of normal donors, non-cancer Nx and Classes II–IV DN patients

Patient characteristics	Normal	Nx	DN Class II	DN Class III	DN Class IV
Age (years)	30.2 ± 17.5	63.4 ± 13.8	51.3 ± 2.5	54.5 ± 13.4	55.47 ± 12.2
SCr (mg/dL)	1.72 ± 1.29	0.89 ± 0.21	2.52 ± 1.79[b]	2.80 ± 1.47[b]	3.83 ± 2.36[b]
UPCR (g/g)	0.59 ± 0.52	0.18 ± 0.08	3.64 ± 3.25	7.47 ± 5.8[a,b]	5.99 ± 4.69
BUN (mg/dL)	N/A	12.97 ± 9.21	27.51 ± 12.19[b]	34.96 ± 15.55[b]	46.26 ± 16.57[b,c]
Blood glucose (mg/dL)	N/A	105.8 ± 22.0	134.9 ± 39.2	211.4 ± 130.0[b]	161.8 ± 82.36
SBP (mmHg)	N/A	134.0 ± 21.5	136.9 ± 18.8	144.0 ± 30.0	160.3 ± 32.2
eGFR (mL/min/1.73 m^2)	100.0 ± 105.4	84.8 ± 17.1	48.3 ± 45.0	27.6 ± 16.0[b]	23.3 ± 18.8[b]

Data are expressed as mean ± SD.
[a]Versus normal.
[b]Versus Nx.
[c]Versus DN Class II, $P < 0.05$.

Table 2. Body weight, blood glucose, GFR and ACR of WT, eNOS$^{-/-}$ and *db/db* eNOS$^{-/-}$ mice

Mouse characteristics	WT	eNOS$^{-/-}$	*db/db* eNOS$^{-/-}$
Body weight (g)	28.03 ± 1.77	25.63 ± 2.60	53.85 ± 5.29[a,b]
Blood glucose (mg/dL)	112.0 ± 8.3	113.7 ± 13.2	376.2 ± 166.7[a,b]
GFR (uL/min/gBW)	12.25 ± 2.03	5.91 ± 2.10[a]	3.64 ± 1.29[a,b]
ACR (ug/mg)	91.6 ± 14.7	146.7 ± 30.3	943.7 ± 265.0[a,b]

Data are expressed as mean ± SD.
[a]Versus WT.
[b]Versus eNOS$^{-/-}$, $P < 0.05$.

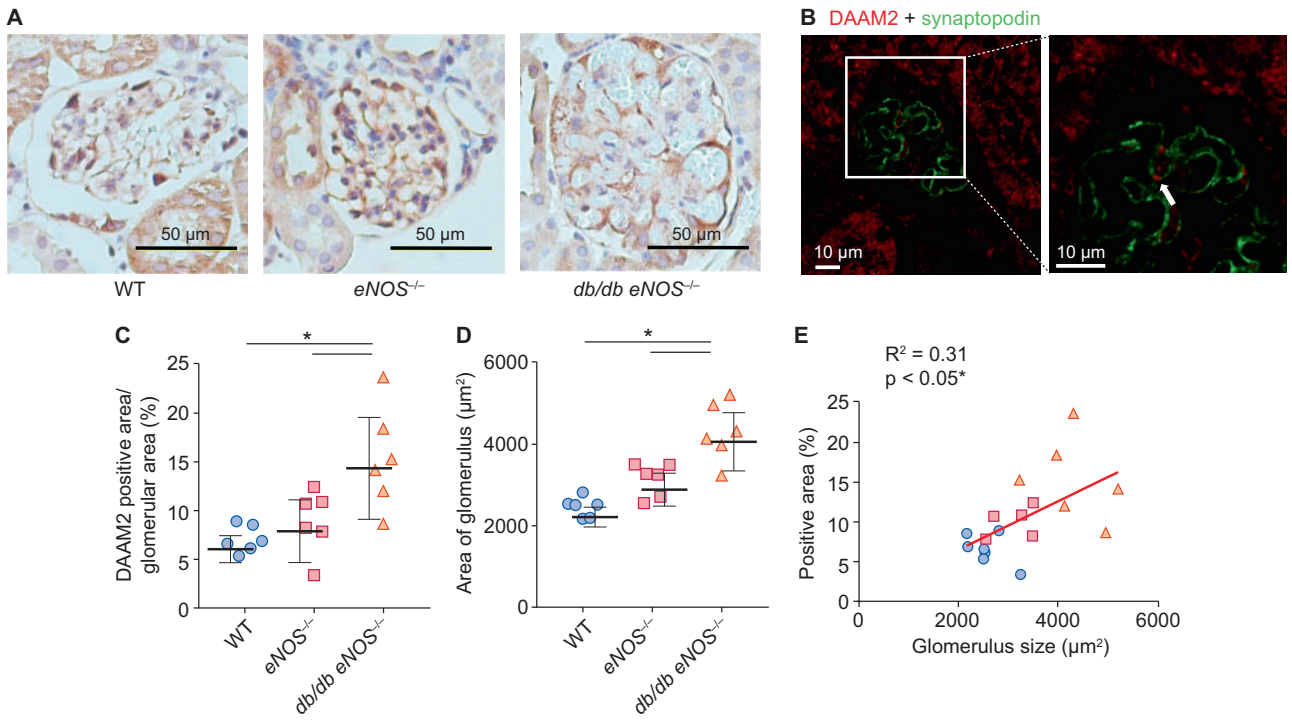

FIGURE 2: Increased podocyte DAAM2 expression in a DN mouse model. (**A**–**C**) Compared with WT and eNOS$^{-/-}$, podocyte DAAM2 expression was increased in *db/db* eNOS$^{-/-}$ (DN) mice. (**D**) Glomerular size increased in DN versus WT and eNOS$^{-/-}$. (**E**) Podocyte DAAM2 expression correlated with glomerular size. * means $p < 0.05$.

the average glomerular size was obtained by averaging scores from all glomeruli on one section.

For immunostaining, microwave treatment was used for antigen retrieval. The sections were quenched with 3% hydrogen peroxide (H_2O_2) in methanol, blocked in 2.5% horse serum and incubated overnight with primary antibody, anti-DAAM2 antibody (Sigma-Aldrich, Darmstadt, Germany). After a phosphate-buffered saline (PBS) rinse, horse radish peroxidase–

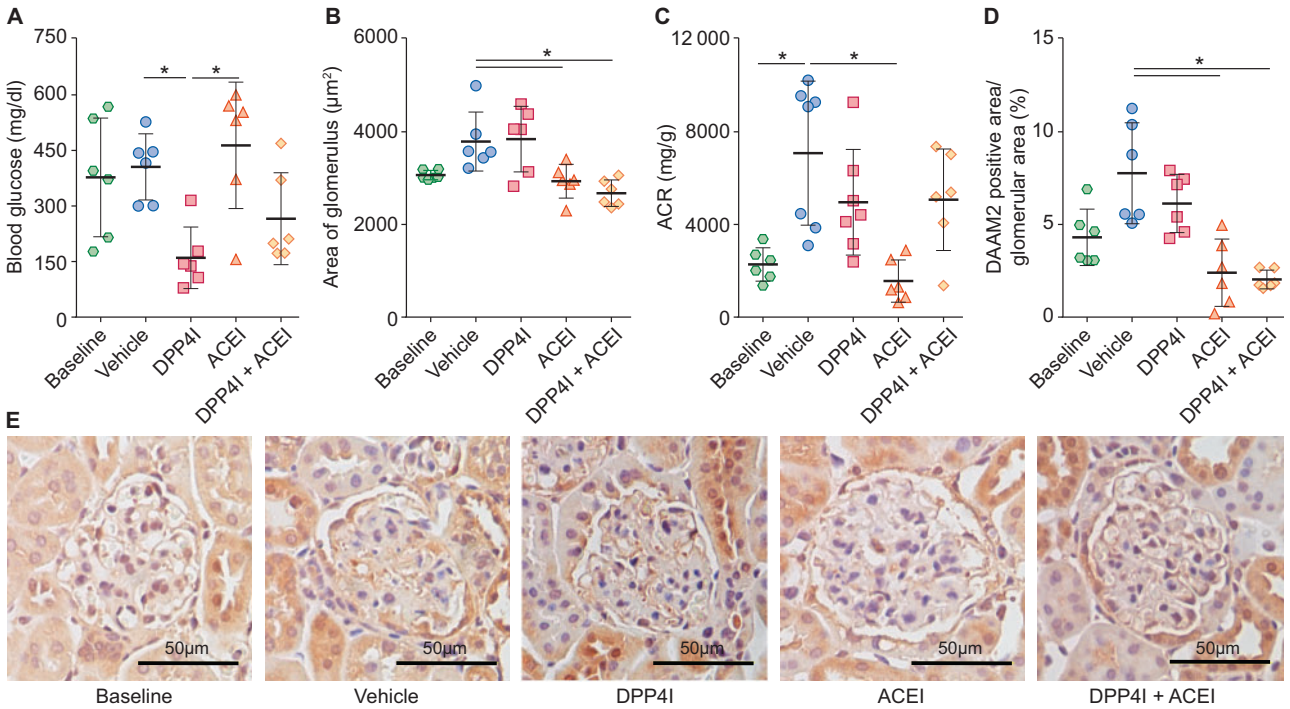

FIGURE 3: Podocyte DAAM2 expression decreased in DN mice treated with ACEI but not in those treated with DPP4I. (**A**) DPP4I reduced blood glucose in DN. (**B**) ACEI, but not DPP4I, reduced glomerular size. (**C**) ACEI reduced urine albumin:creatinine ratio (ACR) in DN. (**D**) ACEI and ACEI + DPP4I but not DPP4I alone reduced podocyte DAAM2 expression. * means $p < 0.05$.

Table 3. Body weight, blood pressure and BUN of sham, uniNx and 5/6 Nx mice

Mouse characteristics	Sham	UniNx	5/6 Nx
Body weight (g)	19.25 ± 1.11	19.40 ± 0.76	18.41 ± 0.77
SBP (mmHg)	93.2 ± 9.0	91.2 ± 4.6	92.6 ± 7.2
BUN (mg/dL)	39.76 ± 3.45	43.40 ± 6.12	56.43 ± 6.93[a,b]

Data are expressed as mean ± SD.
[a]Versus sham.
[b]Versus uniNx, $P < 0.05$.

conjugated secondary antibodies (Vector Labs, Burlingame, CA, USA) were applied for 1 h. 3,3′-Diaminobenzidine (Invitrogen, Carlsbad, CA, USA) was applied for immunohistochemistry. Images were taken using a Zeiss laser scan microscope. At least 25 glomeruli were captured per slide for immunohistochemistry scoring. The mean value of the positive area percentage related to the glomerular area of each slide was analyzed with ImageJ.

For double immunofluorescence staining, the primary antibodies and secondary antibodies were applied following the same protocol as for immunohistochemistry staining. After the secondary antibody, Alexa Fluor Tyramide SuperBoost Kit (Invitrogen) was applied for immunofluorescence staining. After a PBS rinse, 3% H_2O_2 incubation and blocking, the second primary antibody was applied and slides were incubated overnight, followed by second antibody and immunofluorescence staining. Images were taken with a confocal microscope (Zeiss). The primary antibodies used in double staining were anti-DAAM2 antibody (Sigma-Aldrich) and anti-synaptopodin antibody (OriGene Technologies, Rockville, MD, USA).

Primary podocyte culture

Glomeruli were isolated by Dynabeads (Invitrogen) perfusion from 5–8-week-old WT C57BL/6 male mice and plated onto collagen I–coated dishes (Corning, Corning, NY, USA). After 5 days of culture, glomeruli were digested and rinsed to obtain primary podocytes. Podocytes were cultured with medium containing 3t3L1 supernatant [16].

SMARTpool ON-TARGET plus DAAM2 small interfering RNA (siRNA) (Dharmacon, Waltham, MA, USA) was used to knock down DAAM2 expression in podocytes. ON-TARGET plus Non-targeting siRNA (Dharmacon) was used as a control. Delivery of siRNA was achieved following the protocol of Lipofectamine RNAi MAX Transfection Reagent (Thermo Fisher, Carlsbad, CA, USA).

Adhesion assay/detachment assay

For adhesion assays, mouse primary podocytes were cultured in collagen I–coated dishes. After treatments, cells were harvested and plated onto new collagen I–coated 96-well plates. After 30, 60, 180 and 240 min of cultivation, the medium was changed and cells were fixed with 4% PFA in PBS at room temperature for 15 min.

For detachment assays, podocytes were cultured on 96-well plates for 5 days then treated with 0.25% Trypsin-EDTA (Gibco, Carlsbad, CA, USA) for 0, 2.5, 5, 7.5 or 10 min. After adding fresh medium to stop digestion, cells were fixed with PFA.

To analyze the cell quantity in both assays, cells were stained with 0.5% toluidine blue O (Sigma-Aldrich). After washing, cells were treated with 100 uL 1% sodium dodecyl sulfate (KD

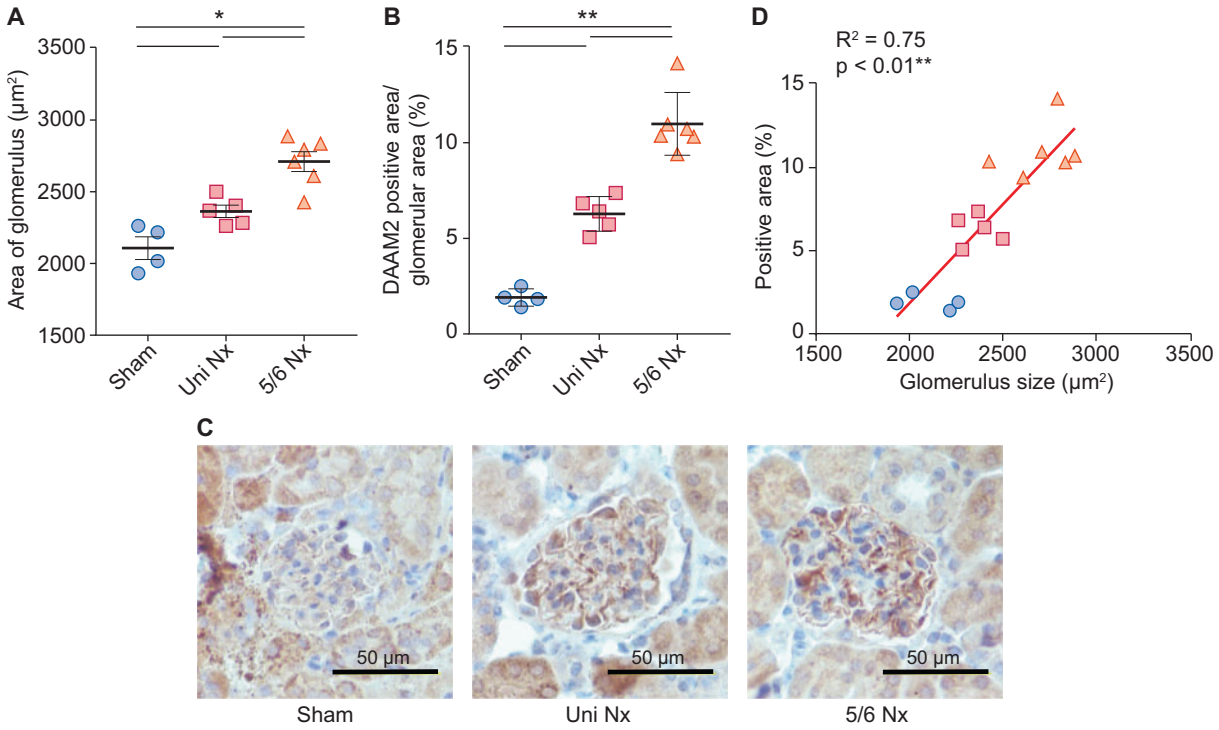

FIGURE 4: Nx-induced glomerular hypertrophy accompanied by enhanced podocyte DAAM2 expression. (**A**) Glomerular size gradually increased in sham, uniNx and 5/6 Nx mice. (**B** and **C**) Podocyte DAAM2 expression also showed similar changes in these three groups. (**D**) Podocyte DAAM2 expression correlated with glomerular size. * means $p < 0.05$ and ** means $p < 0.01$.

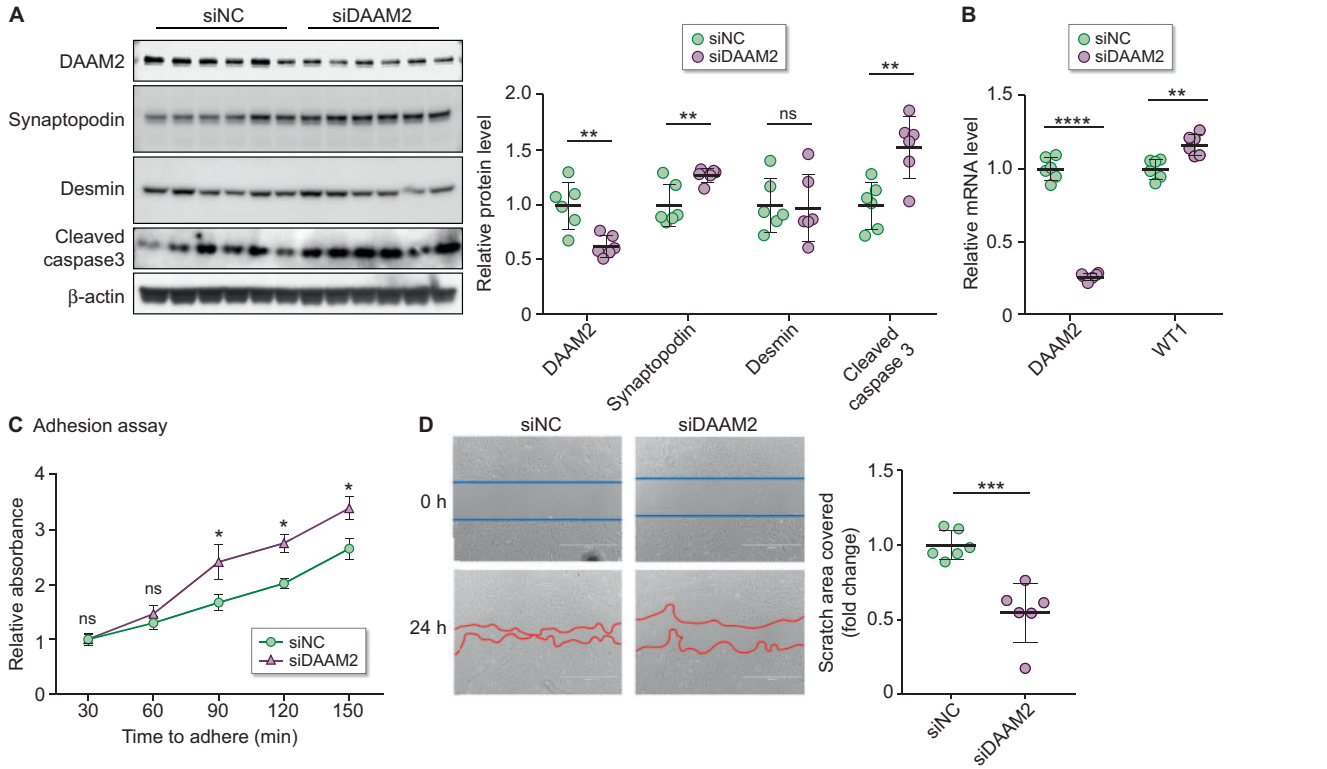

FIGURE 5: DAAM2 knockdown augmented podocyte function. (**A**) DAAM2 was successfully knocked down in primary cultured podocyte by siRNA. Synaptopodin and cleaved caspase-3 increased in DAAM2-KD cells (siDAAM2) versus WT cells (siNC). (**B**) DAAM2 knockdown increased WT1 mRNA. (**C**) DAAM2 knockdown enhanced podocyte adhesion to collagen I–coated plates. (**D**) Migration was reduced in siDAAM2 versus siNC podocytes. * means $p < 0.05$; ** means $p < 0.01$; *** means $p < 0.001$ and **** means $p < 0.0001$.

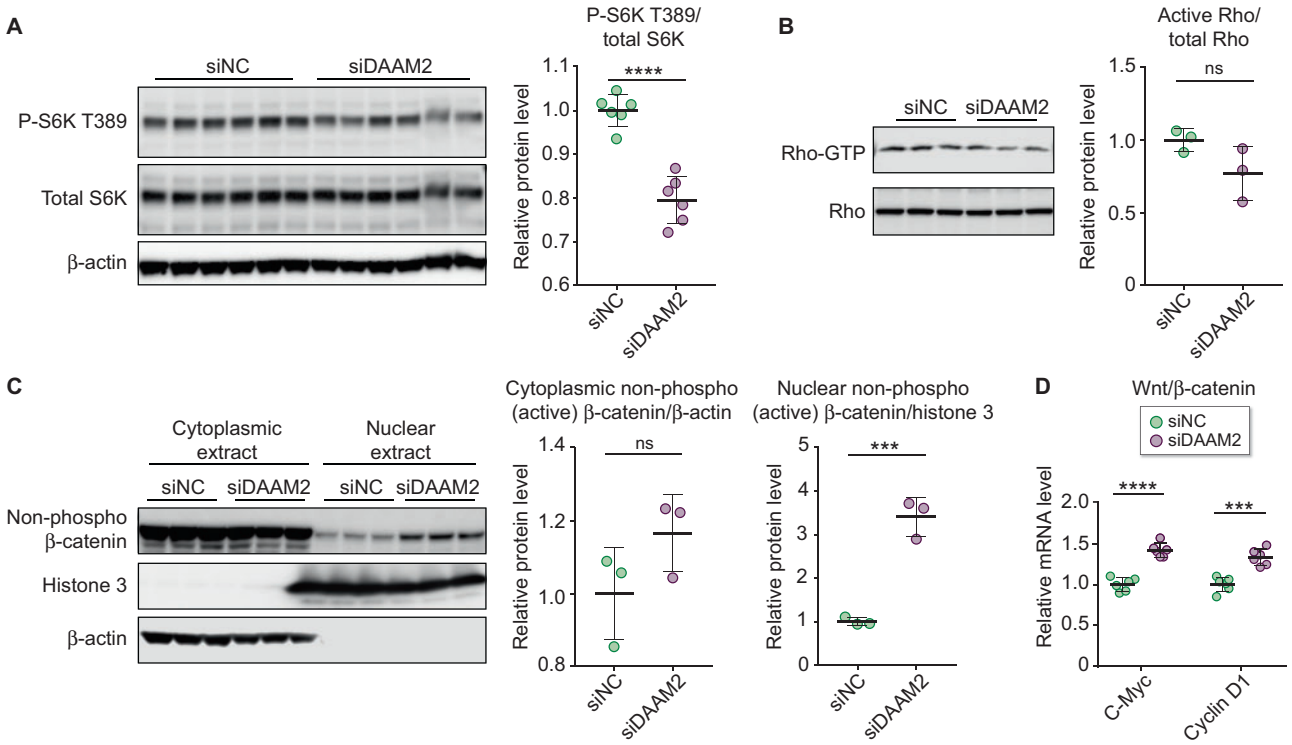

FIGURE 6: DAAM2 expression affected mTOR, Rho and Wnt–β-catenin pathways. (**A**) The ratio of p-S6K T389 to total S6K was reduced in siDAAM2 versus siNC podocytes. (**B**) DAAM2 knockdown numerically reduced GTP-bound Rho (active Rho)/total Rho versus control. (**C**) Nuclear β-catenin was significantly increased in siDAAM2 versus siNC podocytes, while cytoplasmic β-catenin showed a numerical increase in siDAAM2. (**D**) Wnt–β-catenin downstream genes *c-myc* and *cyclin D1* were reduced in siDAAM2 versus siNC podocytes. *** means $p < 0.001$ and **** means $p < 0.0001$.

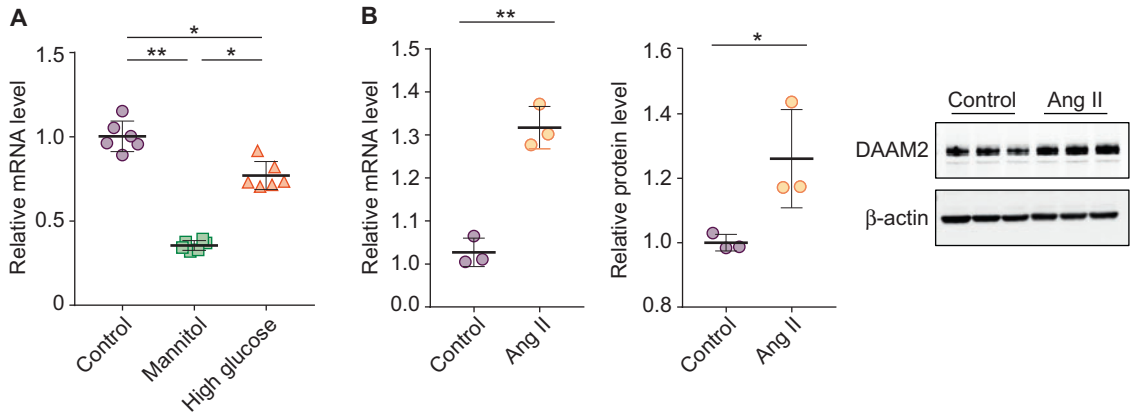

FIGURE 7: Regulation of DAAM2 by high glucose and Ang II. (**A**) Podocyte DAAM2 was markedly decreased in mannitol-treated podocytes, while high glucose resulted in less of a decrease. (**B**) Both protein and mRNA levels of DAAM2 were increased in Ang II–treated podocytes versus controls.

Medical, Columbia, MD, USA). The optical density of each well was measured using a microplate reader (BMG Labtech, Ortenberg, Germany) set to 595 nm. A standard curve was made by a series of standard toluidine blue O samples at a range of concentrations.

Migration assay

Mouse primary podocytes were plated on a collagen I–coated culture dish for 5 days. After transfecting with siRNA (DAAM2-targeting and non-targeting) for 24 h in corresponding wells, two scratches per well were made using 100-uL pipette tips. Wells were washed with Hanks' balanced salt solution followed by a medium change. Baseline (0 h) and 24-h phase-contrast images (4×) were taken with an EVOS inverted microscope. The mean scratch areas of at least six images of each sample and every time point were measured and analyzed with ImageJ software. The scratch area covered from 0 to 24 h of each well was calculated and used to represent the migration ability of each sample.

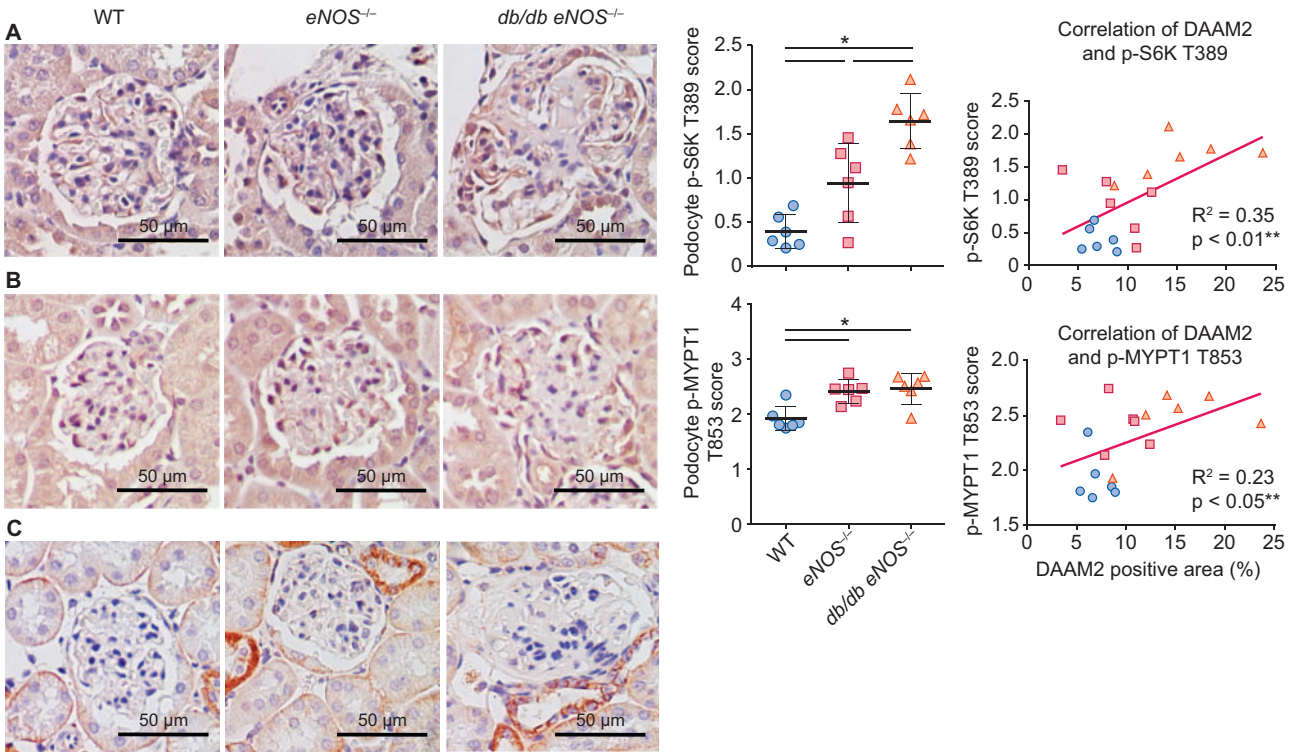

FIGURE 8: Activated mTOR and Rho pathway in DN podocytes. (**A**) Compared with WT and eNOS$^{-/-}$, podocyte p-S6K T389 expression was increased in *db*/*db* eNOS$^{-/-}$ and correlated with DAAM2 expression. (**B**) Compared with WT and eNOS$^{-/-}$, podocyte p-MYPT1 T853 expression was increased in *db*/*db* eNOS$^{-/-}$ and correlated with DAAM2 expression. (**C**) Rare active β-catenin expression in podocytes was detected in all groups.

Real-time polymerase chain reaction (PCR)

Messenger RNA (mRNA) was harvested according to the handbook of the RNeasy Mini Kit (Qiagen, Düsseldorf, Germany). The concentration of RNA was measured with NanoDrop 2000/2000c spectrophotometers (Thermo Fisher). Reverse transcription was done according to the handbook for High-capacity cDNA Reverse Transcription Kits (Applied Biosystems, Foster City, CA, USA). Master mix was prepared for each gene using Universal Master Mix II without UNG (Applied Biosystems) and real-time PCR was performed using a CFX96 system (Bio-Rad, Hercules, CA, USA).

All the primers used were purchased from Thermo Fisher (catalog numbers: DAAM2, Mm01273811_m1; CyclinD1/CCND1, Mm00432359_m1; C-Myc, Mm00487804_m1; Rn18s, Mm03928990_g1).

Western blot analysis

Protein samples were prepared for Western blot analysis by addition of RIPA lysis buffer (Boston BioProducts, Ashland, MA, USA) with subsequent ultrasonic treatment for 5 min. The protein concentration was measured by using a Pierce BCA Protein Assay Kit (Thermo Fisher). Samples were heated to 95°C for 3 min with corresponding volumes of protein loading buffer (4×). Proteins were separated by electrophoresis in precast gradient gels (Invitrogen) in an electrophoresis chamber at 100 V for 2 h and then transferred to nitrocellulose membranes under preset program no. 3 for 7 min (Invitrogen). Membranes were blocked for 1 h at room temperature with 5% powdered non-fat milk in tris-buffered saline and Tween 20 (TBST) and then incubated with primary antibodies overnight at 4°C and secondary antibodies for 1 h at room temperature. Membranes were washed in TBST after incubation with primary or secondary antibodies. Pictures were developed with an Amersham Imager 600 (GE Healthcare, Piscataway, NJ, USA) using Chemiluminescence Substrates (PerkinElmer, Waltham, MA, USA) and analyzed with Image J.

Primary podocytes were plated onto collagen I–coated dishes (Corning) and grown to 70–80% confluency. After treatment, cytoplasmic and nuclear extracts were prepared according to the standard protocol provided by the nuclear extraction kit (Abcam, Cambridge, MA, USA). The protein concentration was measured. Samples were then applied for Western blot analysis. Histone 3 was used as the loading control of the nuclear extract and β-actin as the loading control of the cytoplasmic extract.

Antibodies used are as follows: DAAM2 (Sigma-Aldrich), p70 S6K (Cell Signaling Technology, Danvers, MA, USA), phospho-p70 S6K (Thr389; Cell Signaling Technology), nonphospho (Active) β-catenin (Ser33/37/Thr41; Cell Signaling Technology), histone3 (Abcam), synaptopodin (OriGene Technologies), cleaved caspase-3 (Cell Signaling Technology) and β-actin (Sigma-Aldrich).

Rho activity

Mouse primary podocytes were plated onto the collagen I–coated dishes. After treatment, the cell lysate was harvested by

the lysis/binding/wash buffer provided by the active Rho detection kit (Cell Signaling Technology), following the manufacturer's instructions to assess the GTP-bound form (active) Rho. The Rho activity was assessed by the ratio of active Rho to total Rho.

Statistical analysis

GraphPad Prism version 8.0 (GraphPad Software, San Diego, CA, USA) was utilized to perform all statistics and create graphs. One-way analysis of variance followed by Bonferroni correction, non-parametric test (Kruskal–Wallis) or unpaired *t*-test was used to indicate statistical significance. Linear regression analysis was performed to evaluate the potential correlation of parameters. Results are expressed as mean ± standard deviation (SD). P-values <0.05 were considered significant.

RESULTS

Podocyte DAAM2 is increased in human DN biopsies and Nx specimens

We first investigated the location of renal DAAM2 expression. It was mainly expressed in glomeruli in normal kidney. Double staining of DAAM2 and synaptopodin revealed that DAAM2 was localized outside the linear pattern of synaptopodin with minor colocalization (Figure 1A). DAAM2 surrounded Wilms' tumor 1 (WT1) nuclear staining (Supplementary data, Figure S1A), suggesting it was mostly in podocyte cytoplasm. There was faint DAAM2 staining in parietal epithelial cells and tubular epithelial cells.

Next we compared the glomerular DAAM2 expression by immunohistochemistry staining in DN with non-neoplastic Nx tissues and healthy kidney donor controls. Demographic and renal function data are shown in Table 1. Glomerular DAAM2 was increased in both Nx tissues and DN biopsy tissues (Class II) compared with normal donors. Glomerular DAAM2 was decreased in DN Classes III and IV and correlated with podocyte loss in sclerotic glomeruli (Figure 1B and C). Both Nx and DN showed a larger glomerular tuft size than normal kidney (Figure 1D). Tubular DAAM2 was not significantly different in normal, Nx and DN (Supplementary data, Figure S1B).

Podocyte DAAM2 expression is increased in DN and Nx mouse models and is decreased by ACEI or DPP4 inhibitor

We compared DAAM2 expression in *db/db* eNOS$^{-/-}$ mice, a DN model, with eNOS$^{-/-}$ and WT mice. Compared with eNOS$^{-/-}$ and WT, *db/db* eNOS$^{-/-}$ mice showed significant obesity, hyperglycemia, proteinuria and reduced glomerular filtration rate (GFR) at age 18 weeks (Table 2). Glomerular DAAM2, expressed on podocytes, was increased in *db/db* eNOS$^{-/-}$ mice (Figure 2A–C), accompanied by significant glomerulomegaly compared with either eNOS$^{-/-}$ or WT mice (Figure 2D). No change in tubular DAAM2 was observed. eNOS$^{-/-}$ mice had a larger glomerular size and a trend towards increased podocyte DAAM2 expression versus WT mice. Glomerular DAAM2 expression correlated with glomerular size across all mice (Figure 2E).

In DN mice, ACEI reduced proteinuria and glomerular size and maintained GFR, while DPP4I reduced blood glucose but did not change proteinuria, GFR or glomerular size (Figure 3A–C). ACEI significantly reduced DAAM2 expression in podocytes in DN mice, while DPP4I only numerically reduced DAAM2 (Figure 3D).

To further investigate whether glomerular hypertrophy stimulates DAAM2 expression in podocytes, we studied kidneys in mice after uniNx or 5/6 Nx. At 9 weeks after surgery, blood urear nitrogen (BUN) was significantly increased, with maintained blood pressure and normal blood glucose, in 5/6 Nx mice compared with uniNx and sham-operated mice (Table 3). Notably, glomerular size was increased in 5/6 Nx versus uniNx versus sham-operated mice (Figure 4A). Similarly, podocyte DAAM2, but not tubular DAAM2, also gradually increased with increased glomerular size (Figure 4B and C). Glomerular DAAM2 expression correlated with glomerular size across all mice (Figure 4D).

DAAM2 knockdown augments podocyte function

To investigate whether DAAM2 impacts podocyte function, we knocked down DAAM2 (DAAM2-KD) to ~50% in primary cultured podocytes from normal mice by siRNA (Figure 5A and B). DAAM2 siRNA did not affect the viability of podocytes compared with control siRNA (DAAM2-KD 0.14 ± 0.03 versus WT 0.13 ± 0.03). Podocyte differentiation, revealed by synaptopodin Western blot and WT1 quantitative PCR , was increased in DAAM2-KD cells versus WT cells (Figure 5A and B). Desmin, a marker of podocyte mesenchymal change in response to injury, did not show a significant change. Podocyte apoptosis, assessed by cleaved caspase-3, was increased in DAAM2-KD cells (Figure 5A). Adhesion to collagen type I–coated wells was increased in DAAM2-KD podocytes compared with WT (Figure 5C). However, detachment of differentiated DAAM2-KD podocytes from collagen type I–coated wells was not different versus WT. A wound healing assay revealed a slower migration to close the gap in DAAM2-KD versus WT cells (Figure 5D).

We next evaluated three signaling pathways related to DAAM2. Mammalian target of rapamycin complex 1 (mTORC1), a key complex in the regulation of hypertrophy and a 'gate' of autophagy in response to various nutrients, has been widely reported to be upregulated in podocytes of DN [17]. The ratio of phospho-p70 SK6 (Thr389) to total p70 S6K, which represents the mTORC1 activation state, was decreased in DAAM2-KD versus WT cells (Figure 6A). We next assessed GTP-bound Rho, a measure of the active form of Rho. Rho activity was numerically downregulated in DAAM2-KD podocytes versus WT (Figure 6B). To assess the Wnt–β-catenin pathway, we isolated cytoplasmic and nuclear extracts of podocytes. Nuclear β-catenin was significantly upregulated after DAAM2-KD, while there were no significant differences in the cytoplasmic β-catenin between the two groups (Figure 6C). In addition, genes downstream of β-catenin, *c-myc* and *cyclin D1*, were increased in DAAM2-KD versus WT (Figure 6D).

We also evaluated the effect of high glucose and angiotensin II (Ang II) on podocyte DAAM2 expression. Mannitol reduced

DAAM2 versus controls. While high glucose also showed less DAAM2 than controls, this decrease was less than that seen with mannitol (Figure 7A). In contrast, Ang II stimulated increases in both DAAM2 mRNA and protein in cultured podocytes (Figure 7B).

Finally, we assessed p-S6K T389, p-MYPT1 T853 (a downstream effector protein of Rho) and active β-catenin by immunostaining in mouse DN. Both p-S6K T389 and p-MYPT1 T853 staining was increased in *db*/*db* eNOS$^{-/-}$ mice compared with WT and positively correlated with podocyte DAAM2 expression (Figure 8). Active β-catenin expression in tubules was increased in *db*/*db* eNOS$^{-/-}$ mice versus WT, with only rare expression in podocytes.

DISCUSSION

The underlying pathogenic mechanisms mediating development and progression of human DN are still not well understood [18]. By using proteomic analysis and RNA sequencing, we identified several novel differentially expressed proteins, including DAAM2, which was upregulated in both human and mouse DN versus controls. Studies have reported the role of DAAM2 in the neuromuscular system and embryonic development, but the potential functions of DAAM2 in kidney diseases have not been reported. In this study we show that DAAM2 is mainly expressed on podocytes in the kidney. Its expression is upregulated in early DN and correlated with glomerular hypertrophy. DAAM2 could potentially regulate podocyte apoptosis, adhesion and migration through several cell signaling pathways.

We found that DAAM2 is expressed in tubular epithelial cells in both human and mouse DN and was also detected in primary cultured human tubular epithelial cells and isolated mouse tubular extracts (Supplementary data, Figure S1C). Tubular DAAM2 was not significantly different when comparing normal, Nx and DN human and mouse kidney. Parallel findings were also observed in primary cultured human tubular epithelial cells with mannitol or glucose treatment (Supplementary data, Figure S1D). In glomeruli, we detected DAAM2 expression only on podocytes under both normal and disease conditions, confirmed by synaptopodin and DAAM2 double staining and studies in primary cultured podocytes. Since podocyte damage is an essential component of glomerular injury in DN, we next focused on the potential contribution of DAAM2 in podocyte injury.

We observed reduced DAAM2 expression in severe DN, correlating with a loss of podocytes in sclerotic glomeruli at this stage. In contrast, podocyte DAAM2 expression was increased in early DN at a stage where podocyte number is maintained. This upregulation was parallel to enlargement of glomerular size, which correlates with elevated GFR in the early phase of DN [19]. Further, we found that podocyte DAAM2 is upregulated in Nx patients and mice. The loss of nephrons seen in many kidney diseases can cause hypertrophic stress (glomerular hypertension, hyperfiltration and/or hypertrophy) on the remaining nephrons [20]. However, podocytes are terminally differentiated cells and cannot replicate to increase in proportion to the increased glomerular tuft size. Thus podocytes have to adapt to the mechanical stretching induced by the enlarged glomerular tufts through hypertrophy and cytoskeleton alteration whereas other glomerular cells can adapt by cell proliferation [21, 22]. mTORC1 is a key factor implicated in podocyte hypertrophy. We found that DAAM2 was associated with increased mTORC1 activity in cultured podocytes. In other cells, DAAM2 has been shown to regulate cell differentiation and cytoskeleton [23]. Our data showed ACEI reduced glomerular size, accompanied by a reduction of podocyte DAAM2 expression. Thus we postulate that increased DAAM2 expression on podocytes could be an adaptive reaction to glomerular hypertrophy-related cell stress. Whether diabetes directly or indirectly affects podocyte DAAM2 expression is not clear. *In vivo* we found that DPP4I only numerically reduced podocyte DAAM2 expression without a change in glomerular size. High glucose did not induce upregulation of DAAM2 in cultured podocytes, but Ang II increased podocyte DAAM2 *in vitro* along with reduced DAAM2 by ACEI *in vivo*.

A mismatch of podocyte hypertrophy and glomerular tuft growth results in increased vulnerability to further injury [24]. The contribution of DAAM2 to podocyte injury appears to be complex. In podocin-AA-4E-BP1 transgenic rats, in which podocytes have retarded capacity of mTORC1-mediated hypertrophy in response to growth factor and nutrient signaling, focal segmental glomerulosclerosis developed [25]. Rapamycin, a partial inhibitor of mTORC1, which also reduces renal and glomerular hypertrophic stress, is another potential therapy for DN [26–28]. However, genetic knockout of mTORC1 specifically in mouse podocytes induced proteinuria and glomerulosclerosis [29], suggesting that reducing the glomerular expansion, but not the compensatory cell growth ability of podocytes, slows the progression of chronic kidney disease (CKD) by alleviating the mismatch of podocyte hypertrophy and glomerular tuft growth. Thus we propose that increased podocyte DAAM2 in the early stage of kidney disease may be a protective response to the hypertrophic stress of glomerular enlargement. As the disease progresses, mTORC1 activation caused by the continued adaptive increase in DAAM2 may then aggravate podocyte damage and the disease process.

In addition, Dvl protein, which combines with members of the DAAM family, is a key component of both the Rho and the Wnt–β-catenin signaling pathways. Rho, first discovered to play a role in cell migration and adhesion ∼20 years ago [30], has crucial functions in cytoskeletal architecture, including actin assembly, polymerization, elongation and actomyosin contractility [31]. In our study, Rho activity only numerically decreased after DAAM2 knockdown, accompanied by reduced migration and increased adhesion of podocytes. Rho signaling pathway inhibition, such as Y27632 or Fasudil (inhibitor of ROCK, the key downstream of Rho), has renoprotective effects in a number of models of kidney damage [32–34]. We are the first to report that downregulation of DAAM2 can activate the Wnt–β-catenin pathway in podocytes, with increased apoptosis and synaptopodin expression. The Wnt–β-catenin pathway plays a critical role during kidney development, nephrogenesis and differentiation [35], as well as kidney repair and

regeneration after acute injury [36]. Wnt–β-catenin signaling abnormally activated in podocytes of both human and mouse DN models, as well as various CKDs, can lead to dysfunction, such as apoptosis and decreased viability of podocytes [36, 37]. Therefore our data support that DAAM2 has effects on numerous aspects of podocyte structure and function, including podocyte hypertrophy, migration, adhesion, apoptosis and differentiation via mTORC1, Wnt–β-catenin and Rho signaling pathways.

We further showed that ACEI treatment in DN mice, which reduced the glomerular tuft enlargement and relieved the hypertrophic stress on podocytes, downregulated DAAM2 and decreased proteinuria. Various interventions, such as low calorie intake and rapamycin [25, 38], which slow kidney growth and glomerular enlargement, have protective effects on CKDs. In addition, the sustained adaptive increase of DAAM2 may increase the risks of mTORC1 and Rho–Rock pathway activation, which are important processes in the progression of DN and could induce downstream signaling and podocyte injury [34]. Taken together, these data suggest that interventions that modulate DAAM2, like rapamycin and ACEI, may have renal protective function in CKDs. However, DAAM2 mutations in three unrelated families with steroid-resistant nephrotic syndrome were described [39]. Overexpression of mutant DAAM2 was postulated to lead to podocyte abnormalities. Our *ex vivo* study also showed that knockdown of DAAM2 induces more podocyte apoptosis, suggesting DAAM2 may be necessary for podocyte survival during development. An inducible podocyte-specific DAAM2-KO model may allow further study of the complex and indispensable role of DAAM2 in the function of podocytes.

In conclusion, we have identified a novel protein, DAAM2, that is increased in podocytes of diseased kidneys, including DN and Nx. As an adaptive response of podocytes in hypertrophic glomeruli, DAAM2 is upregulated in early kidney disease. DAAM2 regulates podocyte function through mTORC1, Wnt–β-catenin and Rho signaling pathways. Further studies are needed to clarify the role of DAAM2 in the progression of kidney disease.

SUPPLEMENTARY DATA

Supplementary data are available at ndt online.

FUNDING

This work was supported by the National Institute of Diabetes and Digestive and Kidney Disease (DK103067-01 to R.C.H. and A.B.F.).

AUTHORS' CONTRIBUTIONS

R.C.H, H.Y. and A.B.F. contributed to the research idea and study design. C.Q. and F.H.M.A contributed to data acquisition. C.Q., V.K, H.Y. and A.B.F contributed to data analysis and interpretation. Each author contributed important intellectual content during manuscript drafting or revision.

CONFLICT OF INTEREST STATEMENT

None declared.

REFERENCES

1. Valk EJ, Bruijn JA, Bajema IM. Diabetic nephropathy in humans: pathologic diversity. *Curr Opin Nephrol Hypertens* 2011; 20: 285–289
2. Zelmanovitz T, Gerchman F, Balthazar AP *et al.* Diabetic nephropathy. *Diabetol Metab Syndr* 2009; 1: 10
3. Yang H, Ericsson A, Reznichenko A *et al.* Transcriptomic profile in early vs late stage of murine diabetic nephropathy. Abstract TH-PO679. Presented at the Amercian Society of Nephrol Kidney Week 2017.
4. Habas R, Kato Y, He X. Wnt/Frizzled activation of Rho regulates vertebrate gastrulation and requires a novel Formin homology protein Daam1. *Cell* 2001; 107: 843–854
5. Kida Y, Shiraishi T, Ogura T. Identification of chick and mouse Daam1 and Daam2 genes and their expression patterns in the central nervous system. *Brain Res Dev Brain Res* 2004; 153: 143–150
6. Aspenstrom P. Formin-binding proteins: modulators of formin-dependent actin polymerization. *Biochim Biophys Acta* 2010; 1803: 174–182
7. Lu Y, Zhang Y, Pan MH *et al.* Daam1 regulates fascin for actin assembly in mouse oocyte meiosis. *Cell Cycle* 2017; 16: 1350–1356
8. Yan T, Zhang A, Shi F *et al.* Integrin αvβ3-associated DAAM1 is essential for collagen-induced invadopodia extension and cell haptotaxis in breast cancer cells. *J Biol Chem* 2018; 293: 10172–10185
9. Cui Q, Xie P. Correlation between Daam2 expression changes and demyelination in Guillain–Barre syndrome. *Cell Mol Neurobiol* 2016; 36: 683–688
10. Ajima R, Bisson JA, Helt JC *et al.* DAAM1 and DAAM2 are co-required for myocardial maturation and sarcomere assembly. *Dev Biol* 2015; 408: 126–139
11. Lee HK, Chaboub LS, Zhu W *et al.* Daam2-PIP5K is a regulatory pathway for Wnt signaling and therapeutic target for remyelination in the CNS. *Neuron* 2015; 85: 1227–1243
12. Welsh IC, Thomsen M, Gludish DW *et al.* Integration of left-right Pitx2 transcription and Wnt signaling drives asymmetric gut morphogenesis via Daam2. *Dev Cell* 2013; 26: 629–644
13. Uehara S, Udagawa N, Kobayashi Y. Regulation of osteoclast function via Rho-Pkn3-c-Src pathways. *J Oral Biosci* 2019; 61: 135–140
14. Tervaert TW, Mooyaart AL, Amann K *et al.* Pathologic classification of diabetic nephropathy. *J Am Soc Nephrol* 2010; 21: 556–563
15. Ma LJ, Fogo AB. Model of robust induction of glomerulosclerosis in mice: importance of genetic background. *Kidney Int* 2003; 64: 350–355
16. Krtil J, Platenik J, Kazderova M *et al.* Culture methods of glomerular podocytes. *Kidney Blood Press Res* 2007; 30: 162–174
17. Fogo AB. The targeted podocyte. *J Clin Invest* 2011; 121: 2142–2145
18. Pourghasem M, Shafi H, Babazadeh Z. Histological changes of kidney in diabetic nephropathy. *Caspian J Intern Med* 2015; 6: 120–127
19. Fogo AB. *Fundamentals of Renal Pathology*, 2nd edn. Berlin: Springer, 2014
20. Kriz W, Lehir M. Pathways to nephron loss starting from glomerular diseases Insights from animal models. *Kidney Int* 2005; 67: 404–419
21. Wiggins JE, Goyal M, Sanden SK *et al.* Podocyte hypertrophy, "adaptation," and "decompensation" associated with glomerular enlargement and glomerulosclerosis in the aging rat: prevention by calorie restriction. *J Am Soc Nephrol* 2005; 16: 2953–2966
22. Kriz W. Glomerular diseases: podocyte hypertrophy mismatch and glomerular disease. *Nat Rev Nephrol* 2012; 8: 618–619
23. Lee HK, Deneen B. Daam2 is required for dorsal patterning via modulation of canonical Wnt signaling in the developing spinal cord. *Dev Cell* 2012; 22: 183–196
24. Fukuda A, Chowdhury MA, Venkatareddy MP *et al.* Growth-dependent podocyte failure causes glomerulosclerosis. *J Am Soc Nephrol* 2012; 23: 1351–1363
25. Nishizono R, Kikuchi M, Wang SQ *et al.* FSGS as an adaptive response to growth-induced podocyte stress. *J Am Soc Nephrol* 2017; 28: 2931–2945
26. Lu MK, Gong XG, Guan KL. mTOR in podocyte function: is rapamycin good for diabetic nephropathy? *Cell Cycle* 2011; 10: 3415–3416

27. Huber TB, Walz G, Kuehn EW. mTOR and rapamycin in the kidney: signaling and therapeutic implications beyond immunosuppression. *Kidney Int* 2011; 79: 502–511
28. Bhattacharjee N, Barma S, Konwar N *et al*. Mechanistic insight of diabetic nephropathy and its pharmacotherapeutic targets: an update. *Eur J Pharmacol* 2016; 791: 8–24
29. Godel M, Hartleben B, Herbach N *et al*. Role of mTOR in podocyte function and diabetic nephropathy in humans and mice. *J Clin Invest* 2011; 121: 2197–2209
30. Ridley AJ. Rho GTPase signalling in cell migration. *Curr Opin Cell Biol* 2015; 36: 103–112
31. Ishizaka M, Gohda T, Takagi M *et al*. Podocyte-specific deletion of Rac1 leads to aggravation of renal injury in STZ-induced diabetic mice. *Biochem Biophys Res Commun* 2015; 467: 549–555
32. Bach LA. Rho kinase inhibition: a new approach for treating diabetic nephropathy? *Diabetes* 2008; 57: 532–533
33. Komers R. Rho kinase inhibition in diabetic nephropathy. *Curr Opin Nephrol Hypertens* 2011; 20: 77–83
34. Dai H, Liu Q, Liu B. Research progress on mechanism of podocyte depletion in diabetic nephropathy. *J Diabetes Res* 2017; 2017: 1–10
35. Wang Y, Zhou CJ, Liu Y. Wnt signaling in kidney development and disease. *Prog Mol Biol Transl Sci* 2018; 153: 181–207
36. Zhou D, Tan RJ, Fu H *et al*. Wnt/β-catenin signaling in kidney injury and repair: a double-edged sword. *Lab Invest* 2016; 96: 156–167
37. Bose M, Almas S, Prabhakar S. Wnt signaling and podocyte dysfunction in diabetic nephropathy. *J Investig Med* 2017; 65: 1093–1101
38. Kramer H. Dietary patterns, calories, and kidney disease. *Adv Chronic Kidney Dis* 2013; 20: 135–140
39. Schneider R, Deutsch K, Hoeprich GJ*et al* et al DAAM2 variants cause nephrotic syndrome via actin dysregulation. *Am J Hum Genet* 2020; 107: 1113–1128

Received: 25.6.2020; Editorial decision: 5.1.2021

Nephrol Dial Transplant (2021) 36: 1016–1022
doi: 10.1093/ndt/gfaa039
Advance Access publication 19 March 2020

Immunoglobulin G/albumin staining in tubular protein reabsorption droplets in minimal change disease and focal segmental glomerulosclerosis

Lihong Bu[1], James Mirocha[2] and Mark Haas[3]

[1]Laboratory Medicine and Pathology, University of Minnesota, Minneapolis, MN, USA, [2]Biostatistics Core, Research Institute and General Clinical Research Center, Cedars-Sinai Medical Center, Los Angeles, CA, USA and [3]Pathology and Laboratory Medicine, Cedars-Sinai Medical Center, Los Angeles, CA, USA

Correspondence to: Mark Haas; E-mail: mark.haas@cshs.org

ABSTRACT

Background. Some renal biopsies cannot distinguish minimal change disease (MCD) from primary focal segmental glomerulosclerosis (FSGS) because of inadequate sampling and/or a lack of sampled glomeruli with segmental sclerosis. As protein excretion in MCD has been described as being albumin-selective, we examined whether the ratio of immunoglobulin G (IgG)/albumin staining in protein reabsorption droplets (tPRD) might help distinguish MCD from FSGS.

Methods. Frozen tissue from 144 native renal biopsies from patients with nephrotic syndrome and a diagnosis of MCD or FSGS [73 MCD, 30 FSGS tip variant (FSGS-tip), 38 FSGS-not otherwise specified (FSGS-NOS), 3 FSGS collapsing] was retrospectively stained by direct immunofluorescence for IgG and albumin; none of these samples showed diagnostic lesions of FSGS. IgG and albumin staining of tPRD were graded on a scale of 0 to 3+ based on the distribution and intensity of staining.

Results. Mean (standard deviation) IgG/albumin staining ratios were 0.186 ± 0.239 for MCD, 0.423 ± 0.334 for FSGS-tip ($P = 0.0001$ versus MCD) and 0.693 ± 0.297 for FSGS-NOS ($P < 0.0001$ versus MCD; $P = 0.0001$ versus FSGS-tip). Of 84 biopsies with a ratio ≤0.33, 63 (75%) showed MCD, whereas among 21 with a ratio of 1.0, all but one showed FSGS (15 FSGS-NOS).

Conclusions. In summary, IgG/albumin staining in tPRD was correlated with histologic diagnosis in renal biopsies with MCD and FSGS. A ratio of ≤0.33 was associated with MCD, whereas a ratio of 1.0 was most often seen with FSGS-NOS.

Keywords: focal segmental glomerulosclerosis, IgG/albumin staining ratio, minimal change disease, protein reabsorption droplets, renal biopsy

INTRODUCTION

The glomerular filtration barrier to protein is composed of fenestrated glomerular endothelium, the glomerular basement membrane (GBM) and filtration slits formed by podocyte foot